Zitierweise: *Angew. Chem. Int. Ed.* **2020**, *59*, 17499–17503
Internationale Ausgabe: doi.org/10.1002/anie.202008264
Deutsche Ausgabe: doi.org/10.1002/ange.202008264

Electroluminescence

Achieving Pure Green Electroluminescence with CIEy of 0.69 and EQE of 28.2% from an Aza-Fused Multi-Resonance Emitter

*Yuewei Zhang, Dongdong Zhang, Jinbei Wei, Xiangchen Hong, Yang Lu, Deping Hu, Guomeng Li, Ziyang Liu, Yang Chen, and Lian Duan**

Dedicated to Professor Youqi Tang on the occasion of his 100th birthday

Abstract: *Pure green emitters are essential for realizing an ultrawide color gamut in next-generation displays. Herein, by fusing the difficult-to-access aza-aromatics onto B (boron)–N (nitrogen) skeleton, a hybridized multi-resonance and charge transfer (HMCT) molecule AZA-BN was successfully synthesized through an effective one-shot multiple cyclization method. AZA-BN shows pure green fluorescence with photoluminance quantum yield of 99.7%. The corresponding green device exhibits a maximum external quantum efficiency and power efficiency of 28.2% and 121.7 lm W^{-1}, respectively, with a full width half maximum (FWHM) of merely 30 nm and Commission Internationale de l'Eclairage (CIE) coordinate y of 0.69, representing the purest green bottom-emitting organic light-emitting diode.*

As the color gamut standard for next-generation wide color gamut displays, the Broadcast Service Television 2020 (BT.2020) requires the monochromatic red (R), green (G), and blue (B) primaries with extremely narrow full-width at half-maximum (FWHM). Compared to other colors, the definition of peak emission wavelength and FWHM is more stringent in green, which sets a significant challenge for ultra-pure green emitters.[1] Although well-defined light-emitting diodes (LEDs) based on quantum dot (QD) and perovskite materials have realized emission bands with FWHMs $\leq$ 30 nm in the green region, they still suffer from serious problems concerning cost, efficiency, operational stability, and large-area fabrication.[2] In contrast, organic LEDs (OLEDs) are now commercially used in display panels, of which the emitters have been developed from early fluorescent and phosphorescent dyes to thermally activated delayed fluorescence (TADF) materials, thereby achieving 100% internal quantum efficiency without the use of precious metals.[3] However, owing to the vibronic coupling between the ground state (S_0) and singlet excited state (S_1) as well as the structural relaxation at S_1, large FWHMs of $>$40 nm are usually observed in these emitters.[4]

To suppress emission band broadening, Hatakeyama et al. proposed a molecular design strategy of multi-resonance induced TADF (MR-TADF).[4b,5] In this B (boron)–N (nitrogen) type MR-TADF material system, an extremely small FWHM could be realized because the localization of highest occupied molecular orbital (HOMO) and lowest unoccupied molecular orbital (LUMO) on different atoms could minimize the bonding/antibonding character and suppress the vibrational coupling and relaxation. However, featuring a rigid heterocyclic skeleton on which the HOMO and LUMO are mainly distributed, materials with MR-TADF only show limited intramolecular charge transfer (ICT) characteristics, rendering it quite a challenge to realize color bathochromic shift from the blue region with the prerequisite of small FWMH.[4b,5,6] Until very recently, we have successfully developed the first examples of blue-green MR-TADF emitters by introducing peripheral electron-withdrawing substituents onto carbazole type B–N skeleton to increase the ICT character of the target molecules, which exhibit narrowband electroluminescence (FWHMs: 32–40 nm) with high external quantum efficiencies (EQEs: 20.9–22.7%).[7] It is shown that molecules with the hybridized multi-resonance and charge transfer (HMCT) properties are promising candidates for narrowband emitters with feasible color tunability.

Considering there are only limited molecular skeletons of MR-TADF compounds and the color coordinates of green light are still not ideal, this communication is committed to using HMCT strategy to further regulate the structure, emission wavelength, and FWHM of MR-TADF material to obtain ultra-pure green emission (Scheme 1a). On one hand, for the first time, a novel BN skeleton fused with aromatic rings, which also participate into the multi-resonance effect, was developed. It is believed that this design strategy may open an avenue towards a new kind of MR-TADF compounds with desired properties. On the other hand, an effective one-shot multiple cyclization method was also developed to synthesize MR-TADF molecules fused with the difficult-to-access aza-aromatics and the possible reaction mechanism was detailly clarified and evidenced. As predicted, the final aza-fused MR-TADF emitter (AZA-BN,

[*] Y. Zhang, Dr. D. Zhang, X. Hong, Y. Lu, D. Hu, G. Li, Z. Liu, Y. Chen, Prof. L. Duan
Key Lab of Organic Optoelectronics and Molecular Engineering of Ministry of Education, Department of Chemistry
Tsinghua University, Beijing 100084 (China)
E-mail: duanl@mail.tsinghua.edu.cn
Y. Zhang, Y. Lu, Prof. L. Duan
Center for Flexible Electronics Technology
Tsinghua University, Beijing 100084 (P. R. China)
J. Wei
Beijing National Laboratory for Molecular Sciences
Institute of Chemistry, Chinese Academy of Sciences
Beijing 100049 (P. R. China)
Supporting information and the ORCID identification number(s) for the author(s) of this article can be found under: https://doi.org/10.1002/anie.202008264.

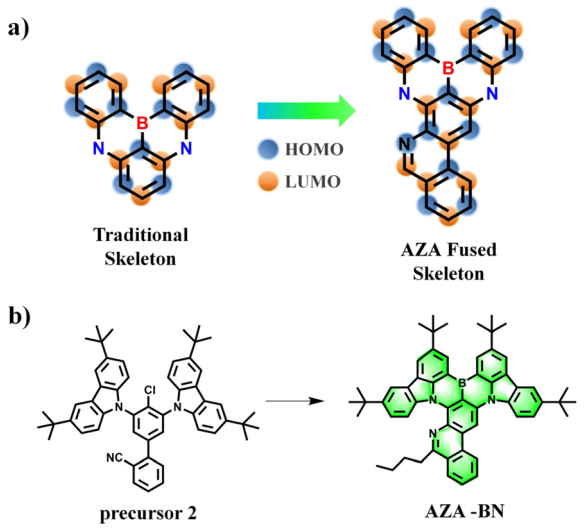

Scheme 1. a) Design of new MR-TADF skeletons with fused aza-aromatics; b) Synthetic procedure: 1) n-BuLi, t-BuPh, 0 °C, 30 min, then 60 °C, 2 h; 2) BBr_3, −40 °C, 0.5 h, then RT, 0.5 h; 3) $NEt(i\text{-}Pr)_2$, 0 °C, then 120 °C, 5 h.

Scheme 1 b) shows pure green emission with a relatively sharp peak at 522 nm, FWHM of 28 nm, and CIEy coordinate of 0.69. Moreover, as aza-aromatics have various interesting properties of π-systems, such as easy electron injection, stable electron transport, strong electron acceptor, high triplet state, facilitated n-type doping and strong affinity for DNA,[8,9a] we think the introduction of aza-aromatics to MR-TADF system should be a very important topic in both synthetic chemistry and organic functional materials.

Our synthetic strategy of the aza-fused MR-TADF molecule is to perform a one-shot multiple cyclization by cleverly combining the imino nitrogen-centered radical-based cyclization with bora-Friedel–Crafts-type reactions.[9] As shown in Scheme 1 a and the Supporting Information, Schemes S1, S2, the key precursor **2** was prepared by a palladium catalyzed Suzuki coupling reaction of the 2-cyanophenylboronic acid with the precursor **1**, which was easily prepared by an aromatic nucleophilic substitution reaction between the fluoroarene and 3,6-diterbutyl carbazole with good yields. During the initial screening of the ratios of precursor **2** to n-butyllithium (n-BuLi), we found that reaction with 1 and 2 equiv of n-BuLi did not give the desired product (AZA-BN), but 4Cl-t-BCz-Ph-2CN and 4Cl-t-BCz-AZA (Supporting Information, Scheme S3 and Figures S1–S4), respectively. This indicates that in the reaction of the intermediate **2** with n-BuLi, the addition of CN and n-BuLi occurs prior to substitution of halogen atom. After extensive screening, it was finally confirmed that the mixture of precursor **2** (1 equiv) and n-BuLi (3 equiv) can successfully synthesize the target HMCT molecule (yield: 20 %). A possible reaction pathway for the present one-pot multiple cyclization reaction of precursor **2** is shown in the Supporting Information, Scheme S4. Intermediate **2** first reacts with n-BuLi to form an imino anion, then the excess n-BuLi will continue to undergo lithium halogen exchange reaction with chlorine. Subsequent treatment with BBr_3 gave intermediate **X** (N-bromine Imine; Supporting Information, Scheme S4) and in the presence of Hünig's base, the intramolecular electrophilic boronation, cyclization of imino nitrogen-centered radical, and oxidation reactions would take place at 120 °C to give the target AZA-BN molecule. Notably, other lithium reagents, such as phenyl lithium and tert-Butyllithium, did not give any aza-fused MR-TADF molecules at all. Moreover, the final product AZA-BN is well soluble in common organic solvents, such as n-hexane, toluene, tetrahydrofuran, and dichloromethane, and shows excellent light and oxygen stability as determined by the repeated photophysical measurements under ambient conditions in which no spectral change is observed.

The single crystal of AZA-BN was successfully grown from CH_2Cl_2/MeOH, so that its structure was unambiguously determined by single-crystal X-ray analysis. As depicted in Figure 1 a, the C38–N2 bond length is 1.31 Å, indicating

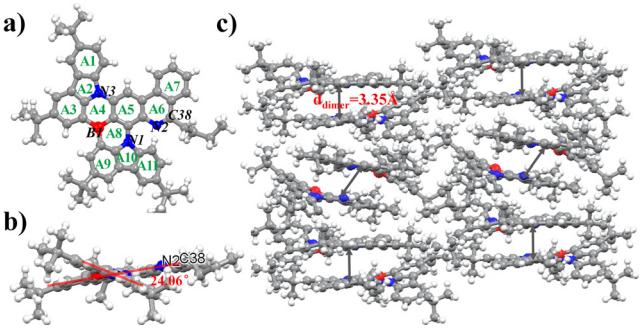

Figure 1. Crystal structure of AZA-BN. a) Top view. b) Side view. c) Crystal packing structure.

a double bond character. The B–C bond length is around 1.54 Å, a typical value for three-coordinated boron-carbon compounds. Rings A1 to A7 lie on one plane and rings A9 to A11 lie on the other plane. The dihedral angles of the two planes are determined to be 24.06° and this special twisted conformation of AZA-BN could be assigned to the large steric hindrance between A6 and A11, which is conducive to enhancing the ICT characteristic (Figure 1 b). Additionally, though this aza-fused MR-TADF molecule adopts a twisted conformation, the B and N (N1 and N3) atoms reside in a planar sp^2-bonding configuration, which is similar to the reported BN-doped graphenes.[5c] In crystal, a notable feature is that AZA-BN molecules aggregate into dimers based on strong intermolecular π···π stacking interactions between the planes consisting of A1 to A7 rings, and the interplanar separation distance and overlapping area are around 3.35 Å and 60 %, respectively (Figure 1 c).

To illustrate the effect of variation of the skeleton on the geometric and optoelectronic properties, time-dependent density functional theory (TD-DFT) using B3LYP(6–31g) method was performed, and the optimized geometry, the HOMO/LUMO distributions, S_1 values, FWHM values, and oscillator strengths are depicted in Figure 2. The DFT optimized geometry of AZA-BN is in good agreement with its crystal, also showing a twisted conformation (Supporting

	MR-TADF		HMCT-TADF	
			Acceptor	Fused acceptor
Structure	DABNA-1	BCz-BN	2F-BN	AZA-BN
HOMO	Reference		No changes	Changes in HOMO distribution
LUMO	Reference		Changes in LUMO distribution	Changes in LUMO distribution
S_1 (eV)	3.13	2.86	2.81	2.64
FWHM(nm)	15	16	17	20
f	0.2046	0.4125	0.4113	0.2820

Figure 2. The molecular structures, HOMO/LUMO distributions, singlet energies, FWHM values, and oscillator strengths of the compounds.

Information, Figure S8). The LUMO is mainly localized on the boron atom as well as its *ortho*/*para* positions in rings A2 to A7 and A8 to A10, while the HOMO is mainly localized on the nitrogen atoms as well as the *meta* position of boron atom in rings A1 to A6 and A8 to A11. Consequently, the introduction of fused aza-aromatics could not only increase the π-conjugated length, but also tune the distributions of HOMO and LUMO simultaneously (compared to BCz-BN), which obviously enhances the ICT character of MR-TADF emitter for small S_1 value and thus red-shifts the emission. Since the fused aza-aromatics could participate into the multi-resonance effect, it is fair to assume that a unique small FWHM of AZA-BN could be maintained (Supporting Information, Figure S9 and Tables S1, S2). It should also be noted that even a higher f value (compared to DABNA-1) was observed for AZA-BN at the same time, attesting the superiority of the molecular design strategy of HMCT. The above results were also well supported by natural transition orbitals (NTOs) for the S_1 and T_1 excitations (Supporting Information, Figure S10 and Table S3). Moreover, the density functional calculations provided the dissociation energies (BDEs) of the C–C single bonds (in N-butyl) as 3.85 eV for **1**, 2.96 eV for **2**, 3.57 eV for **3**, and 3.74 eV for **4**, which is much higher than that of S_1 (2.64 eV) and T_1 (2.23 eV) excited state energies, indicating the stability of C–C bonds in AZA-BN (Supporting Information, Figure S11).[10]

The UV/Vis absorption and emission spectra of AZA-BN in various solvents with different polarities were shown in the Supporting Information, Figure S12 and the photophysical data were summarized in Table 1. The strong absorption bands peaking at around 500 nm were assigned to the ICT absorption transitions. Compared to the typical MR-TADF emitter DABNA-1, AZA-BN displayed a more significant solvatochromic effect with remarkable red-shifts and stokes shifts/FWHMs broadening upon altering the solvents from weak (n-hexane) to strong (dichloromethane) polarity, which can be assigned to the more separated HOMO–LUMO distributions.[5a] Nevertheless, the maximum stokes shift of 24 nm and FWHM of 34 nm are still very small and the emissions (λ_{em}:512–528 nm) are much red-shifted than the reported MR-TADF emitters, evidencing the superiority of the molecular design strategy of HMCT in exploring highly efficient TADF emitters with the narrow and full-color emissions. Notably, as shown in Figure 3, the CIE coordinates of AZA-BN in toluene is (0.23, 0.69), which perfectly satisfies the pure green requirements of (0.21, 0.71) defined by the National Television System Committee (NTSC). Benefitting from the higher f value, the absolute quantum yield (Φ) determined with an integer-sphere system in degassed toluene solution is substantially higher than that of DABNA-1, almost to 100% (99.7%). The phosphorescence spectrum at 77 K shows an emission band maximum at $\lambda = 567$ nm (Figure 3). Combined with the fluorescence emission wavelength of 522 nm, the energy difference between the excited singlet and triplet states (ΔE_{ST}) is estimated to be 0.18 eV.

The photophysical properties of AZA-BN in doped film were also recorded with 3,3′-bis(*N*-carbazolyl)-1,1′-biphenyl (mCBP) as the wide energy gap host. As depicted in the Supporting Information, Figure S14, the 4 wt% AZA-BN:mCBP doped film also gave a near-pure green emission

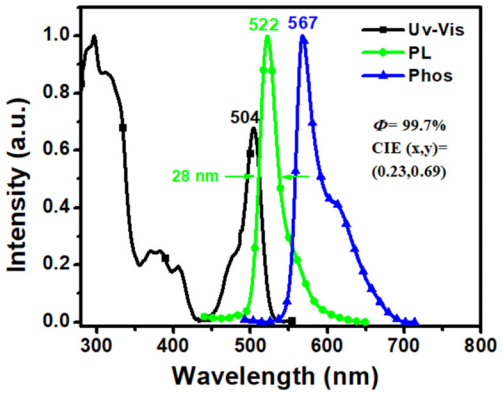

Figure 3. UV/Vis absorption, fluorescence (298 K), and phosphorescence (77 K) spectra of AZA-BN in toluene.

Table 1: Photophysical data of AZA-BN.

	S_1[a] [eV]	T_1[a] [eV]	ΔE_{ST}[a] [eV]	FWHM[a] [nm]	HOMO[b] [eV]	LUMO[c] [eV]	PLQY[d]	τ_{PF}[d] [ns]	τ_{DF}[d] [ms]	k_r [$\times 10^7\ s^{-1}$][d]	k_{ISC} [$\times 10^7\ s^{-1}$][d]	k_{RISC} [$\times 10^3\ s^{-1}$][d]
AZA-BN	2.37	2.19	0.18	28	−5.07	−2.73	94%	13.4	0.16	5.04	2.42	7.53

[a] Measured in the toluene solution with a concentration of 10^{-5} mol L^{-1}. [b] Deduced from LUMO and energy gap (E_g) values. [c] Measured in dry N,N-dimethylformamide with a concentration of 10^{-3} mol L^{-1}. [d] Measured in 4 wt%-doped films of AZA-BN in mCBP.

with emission maximum at 526 nm and CIE coordinates of (0.25, 0.70). The emission peak of the doped film was slightly broadened (FWHM = 36 nm) and the Φ value was 0.94, probably due to the existence of π–π interactions between the dopants, or dopant and host, and the conformational change. The quantum yields ($\Phi_{PF} = 0.68$ and $\Phi_{DF} = 0.26$) and lifetimes ($\tau_{PF} = 13.4$ ns and $\tau_{DF} = 160$ μs) of the fluorescence and TADF components can be estimated from the total Φ and ratio of the integrated area of each component in the transient spectra to the total integrated area (Supporting Information, Figures S15, S16).[3j] Notably, a large rate constant of fluorescence (k_r) value of 5.04×10^7 s^{-1} was determined based on the Φ_{PF} and τ_{PF} values, which is much higher than most of the reported TADF emitters.[11] These are promising characteristics of TADF dye for fabricating OLED with high efficiency and color purity.

To demonstrate the potential of aza-fused MR-TADF molecule, a phosphorescence sensitized thermally activated delayed fluorescent (PSTADF) OLED[12] employing AZA-BN as the emitter was fabricated with the following structure (see the Supporting Information for the non-sensitized devices): indium tin oxide (ITO)/1,4,5,8,9,11-hexaazatriphenylene hexacarbonitrile (HATCN) (10 nm)/4,4′-N,N′-bis[N-(1-naphthyl)-N-phenylamino]biphenyl (NPB) (30 nm)/9,9′-Diphenyl-9*H*,9′*H*-3,3′-bicarbazole (BCzPh) (10 nm)/mCBP:30 wt % $Ir(ppy)_3$:6 wt % AZA-BN (18 nm)/4,6-bis(3-(9*H*-carbazol-9-yl)phenyl)pyrimidine (CzPhPy) (10 nm)/9,10-bis(6-phenylpyridin-3-yl)anthracene (DPPyA) (30 nm)/LiF (0.5 nm)/Al (150 nm). The energy diagram[13] and chemical structures of the materials used in this device are shown in Figure 4a, detailed device performances are depicted in Figures 4b,c and the Supporting Information, Figure S17. The device shows a low turn-on voltage (V_{on}, at 1 cd m^{-2}) of 2.6 V, and near-pure green emission with a relatively sharp peak at 527 nm, FWHM of 30 nm, and CIE coordinates of (0.27, 0.69). To the best of our knowledge, such high green-light color purity represents the purest green emission ever reported in OLEDs, revealing the superiority of HMCT strategy in achieving the ultra-pure green EL.[14] The device shows high efficiencies with maximum EQE (EQE_{max}) and power efficiency (PE_{max}) of 28.2 % and 121.7 lm W^{-1}, respectively, which are among the best performance values reported for green OLEDs. It is worth noting that the power efficiency here set a new record for all fused N/B systems.[5–7,12,15] Furthermore, the device also shows a small efficiency roll-off with EQE remaining at 26.5 % and 19.1 % under brightness of 100 cd m^{-2} and 1000 cd m^{-2}, respectively. Time to 90 % of the initial luminance (T90) was measured to be 46.3 h at a high brightness of 2000 cd m^{-2}, testifing the stability of AZA-BN emitter (Supporting Information, Figure S19).

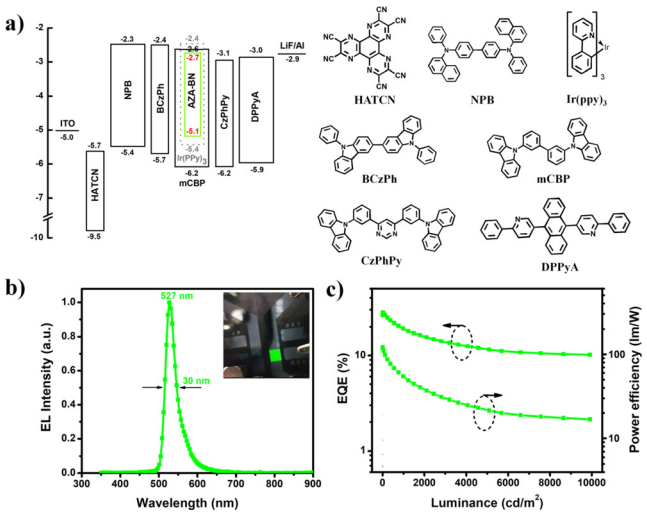

Figure 4. a) The energy level diagram of the device and the molecule structures of the materials used in this device. b) Normalized EL spectra and device in operation. c) The EQE-luminance-power efficiency curves of the AZA-BN based device.

In summary, by fusing aza-aromatics onto BN skeleton, a novel HMCT molecule AZA-BN was successfully synthesized through a one-shot multiple cyclization reaction. DFT calculations showed that the aza-aromatics could participate into the multi-resonance, which will greatly enrich the types of MR-TADF skeletons. The target molecule AZA-BN shows near pure green emission with a relatively sharp peak at 522 nm, FWHM of 28 nm, and extremely high Φ of 99.7 %. The corresponding green device exhibits a maximum external quantum efficiency and power efficiency of 28.2 % and 121.7 lm W^{-1}, respectively, with FWHM of merely 30 nm and CIE coordinate *y* of 0.69, representing the purest green bottom-emitting organic light-emitting diode. We believe our molecular design and synthesis strategy of fusing aromatic rings onto BN skeleton would continue to guide the exploration of highly efficient MR-TADF emitters with full-color emissions.

Acknowledgements

This work was supported by the National Key Basic Research and Development Program of China (Grant No. 2016YFB0401003), the National Science Fund of China (Grant Nos. 51525304, and 61890942), the China Postdoctoral Science Foundation (Grant No. 2019M650628) and Foshan Xianhu Laboratory of the Advanced Energy Science and Technology Guangdong Laboratory XHT2020-005.

Conflict of interest

The authors declare no conflict of interest.

Keywords: electroluminiscence · fused aza-aromatics · hybridized multi-resonance and charge transfer · pure green emission

[1] a) J. S. Steckel, J. Ho, S. Coe-Sullivan, *Photonics Spectra* **2014**, *48*, 55 – 61; b) D. J. Yu, F. Cao, Y. J. Gao, Y. H. Xiong, H. B. Zeng, *Adv. Funct. Mater.* **2018**, *28*, 1800248.

[2] a) H. Cho, S. H. Jeong, M. H. Park, Y. H. Kim, C. Wolf, C. L. Lee, J. H. Heo, *Science* **2015**, *350*, 1222; b) S. Kumar, J. Jagielski, N. Kallikounis, Y.-H. Kim, C. Wolf, F. Jenny, T. Tian, C. J. Hofer,

Y.-C. Chiu, W. J. Stark, T.-W. Lee, C.-J. Shih, *Nano Lett.* **2017**, *17*, 5277.

[3] a) C. W. Tang, S. A. Vanslyke, *Appl. Phys. Lett.* **1987**, *51*, 913; b) M. A. Baldo, D. F. O'Brien, Y. You, A. Shoustikov, S. Sibley, M. E. Thompson, S. R. Forrest, *Nature* **1998**, *395*, 151; c) K. Kim, C. Moon, J. Lee, S. Kim, J. Kim, *Adv. Mater.* **2014**, *26*, 3844; d) H. Uoyama, K. Goushi, K. Shizu, H. Nomura, C. Adachi, *Nature* **2012**, *492*, 234; e) S. Y. Lee, T. Yasuda, Y. S. Yang, Q. Zhang, C. Adachi, *Angew. Chem. Int. Ed.* **2014**, *53*, 6402 – 6406; *Angew. Chem.* **2014**, *126*, 6520 – 6524; f) Y. Tao, K. Yuan, T. Chen, P. Xu, H. Li, R. Chen, C. Zheng, L. Zhang, W. Huang, *Adv. Mater.* **2014**, *26*, 7931; g) L.-S. Cui, H. Nomura, Y. Geng, J. U. Kim, H. Nakanotani, C. Adachi, *Angew. Chem. Int. Ed.* **2017**, *56*, 1571 – 1575; *Angew. Chem.* **2017**, *129*, 1593 – 1597; h) J.-X. Chen, K. Wang, C.-J. Zheng, M. Zhang, Y.-Z. Shi, S.-L. Tao, H. Lin, W. Liu, W.-W. Tao, X.-M. Ou, X.-H. Zhang, *Adv. Sci.* **2018**, *5*, 1800436; i) D. Zhang, X. Song, M. Cai, H. Kaji, L. Duan, *Adv. Mater.* **2018**, *30*, 1705406; j) I. S. Park, K. Matsuo, N. Aizawa, T. Yasuda, *Adv. Funct. Mater.* **2018**, *28*, 1802031; k) Y. Liu, C. Li, Z. Ren, S. Yan, M. R. Bryce, *Nat. Rev. Mater.* **2018**, *3*, 18020; l) W. Li, B. Li, X. Cai, L. Gan, Z. Xu, W. Li, K. Liu, D. Chen, S.-J. Su, *Angew. Chem. Int. Ed.* **2019**, *58*, 11301 – 11305; *Angew. Chem.* **2019**, *131*, 11423 – 11427; m) W. Zeng, T. Zhou, W. Ning, C. Zhong, J. He, S. Gong, G. Xie, C. Yang, *Adv. Mater.* **2019**, *31*, 1901404.

[4] a) F. Santoro, A. Lami, R. Improta, J. Bloino, V. Barone, *J. Chem. Phys.* **2008**, *128*, 224311; b) Y. Kondo, K. Yoshiura, S. Kitera, H. Nishi, S. Oda, H. Gotoh, Y. Sasada, M. Yanai, T. Hatakeyama, *Nat. Photonics* **2019**, *13*, 678 – 682.

[5] a) T. Hatakeyama, K. Shiren, K. Nakajima, S. Nomura, S. Nakatsuka, K. Kinoshita, J. Ni, Y. Ono, T. Ikuta, *Adv. Mater.* **2016**, *28*, 2777 – 2781; b) S. Nakatsuka, H. Gotoh, K. Kinoshita, N. Yasuda, T. Hatakeyama, *Angew. Chem. Int. Ed.* **2017**, *56*, 5087; *Angew. Chem.* **2017**, *129*, 5169; c) K. Matsui, S. Oda, K. Yoshiura, K. Nakajima, N. Yasuda, T. Hatakeyama, *J. Am. Chem. Soc.* **2018**, *140*, 1195 – 1198; d) S. Oda, B. Kawakami, R. Kawasumi, R. Okita, T. Hatakeyama, *Org. Lett.* **2019**, *21*, 9311 – 9314.

[6] a) X. Liang, Z.-P. Yan, H.-B. Han, Z.-G. Wu, Y.-X. Zheng, H. Meng, J.-L. Zuo, W. Huang, *Angew. Chem. Int. Ed.* **2018**, *57*, 11316 – 11320; *Angew. Chem.* **2018**, *130*, 11486 – 11490; b) Y. Yuan, X. Tang, X.-Y. Du, Y. Hu, Y.-J. Yu, Z.-Q. Jiang, L.-S. Liao, S.-T. Lee, *Adv. Opt. Mater.* **2019**, *7*, 1801536; c) J. A. Knöller, G. Meng, X. Wang, D. Hall, A. Pershin, D. Beljonne, Y. Olivier, S. Laschat, E. Zysman-Colman, S. Wang, *Angew. Chem. Int. Ed.* **2020**, *59*, 3156 – 3160; *Angew. Chem.* **2020**, *132*, 3181 – 3185; d) Y. Xu, Z. Cheng, Z. Li, B. Liang, J. Wang, J. Wei, Z. Zhang, Y. Wang, *Adv. Opt. Mater.* **2020**, *8*, 1902142.

[7] Y. Zhang, D. Zhang, J. Wei, Z. Liu, Y. Lu, L. Duan, *Angew. Chem. Int. Ed.* **2019**, *58*, 16912; *Angew. Chem.* **2019**, *131*, 17068.

[8] a) J. E. Anthony, A. Facchetti, M. Heeney, S. R. Marder, X. Zhan, *Adv. Mater.* **2010**, *22*, 3876; b) Y. Min, C. Dou, D. Liu, H. Dong, J. Liu, *J. Am. Chem. Soc.* **2019**, *141*, 17015 – 17021.

[9] a) A. Kishi, K. Moriyama, H. Togo, *J. Org. Chem.* **2018**, *83*, 11080 – 11088; b) H. Narutoa, H. Togo, *Org. Biomol. Chem.* **2019**, *17*, 5760 – 5770; c) E. Kobayashi, A. Kishi, H. Togo, *Eur. J. Org. Chem.* **2019**, 7335 – 7347; d) H. Hirai, K. Nakajima, S. Nakatsuka, K. Shiren, J. Ni, S. Nomura, T. Ikuta, T. Hatakeyama, *Angew. Chem. Int. Ed.* **2015**, *54*, 13581 – 13585; *Angew. Chem.* **2015**, *127*, 13785 – 13789.

[10] a) N. Lin, J. Qiao, L. Duan, H. Li, L. Wang, Y. Qiu, *J. Phys. Chem. C* **2012**, *116*, 19451 – 19457; b) D. Y. Kondakov, *J. Appl. Phys.* **2008**, *104*, 084520.

[11] K. Sato, K. Shizu, K. Yoshimura, A. Kawada, H. Miyazaki, C. Adachi, *Phys. Rev. Lett.* **2013**, *110*, 247401.

[12] K. H. Lee, J. Y. Lee, *J. Mater. Chem. C* **2019**, *7*, 8562.

[13] a) B. B. Diouf, W. S. Jeon, J. S. Park, J. W. Choi, Y. H. Son, D. C. Lim, Y. J. Doh, J. H. Kwon, *Synth. Met.* **2011**, *161*, 2087; b) J. K. Bin, N. S. Cho, F. J. I. Hong, *Adv. Mater.* **2012**, *24*, 2911; c) M. Mamada, G. J. Tian, H. Nakanotani, J. H. Su, C. Adachi, *Angew. Chem. Int. Ed.* **2018**, *57*, 12380; *Angew. Chem.* **2018**, *130*, 12560; d) Z. Liu, M. G. Helander, Z. Wang, Z. Lu, *Org. Electron.* **2013**, *14*, 852; e) C. Cai, S. J. Su, T. Chiba, H. Sasabe, Y. J. Pu, K. Nakayama, J. Kido, *Jpn. J. Appl. Phys.* **2011**, *50*, 040204; f) D. D. Zhang, J. Qiao, D. Q. Zhang, L. Duan, *Adv. Mater.* **2017**, *29*, 1702847.

[14] a) P. Rajamalli, N. Senthilkumar, P. Gandeepan, P. Y. Huang, M. J. Huang, C. Z. Ren-Wu, C. Y. Yang, M. J. Chiu, L. K. Chu, jH. W. Lin, C. H. Cheng, *J. Am. Chem. Soc.* **2016**, *138*, 628; b) M. Y. Wong, E. Zysman-Colman, *Adv. Mater.* **2017**, *29*, 1605444; c) H. Fukagawa, T. Oono, Y. Iwasaki, T. Hatakeyama, T. Shimizu, *Mater. Chem. Front.* **2018**, *2*, 704; d) T.-L. Wu, M.-J. Huang, C.-C. Lin, P.-Y. Huang, T.-Y. Chou, R.-W. Chen-Cheng, H.-W. Lin, R.-S. Liu, C.-H. Cheng, *Nat. Photonics* **2018**, *12*, 235.

[15] a) S. H. Han, J. H. Jeong, J. W. Yoo, J. Y. Lee, *J. Mater. Chem. C* **2019**, *7*, 3082 – 3089; b) T. B. Nguyen, H. Nakanotani, T. Hatakeyama, C. Adachi, *Adv. Mater.* **2020**, *32*, 1906614.

Manuscript received: June 10, 2020
Accepted manuscript online: July 2, 2020
Version of record online: August 11, 2020

